Author(s): Karttunen, Anssi T. & von Hertzen, Raimo

Title: Polymer cover induced self-excited vibrations of nipped rolls

Year: 2011

Version: Post print

Please cite the original version:

Karttunen, Anssi T. & von Hertzen, Raimo. 2011. Polymer cover induced self-excited vibrations of nipped rolls. Journal of Sound and Vibration. Volume 330, Issue 16. 3959-3972. ISSN 0022-460X (printed). DOI: 10.1016/j.jsv.2011.03.016.

Polymer cover induced self-excited vibrations of nipped rolls[†]

Anssi T. Karttunen[a,*], Raimo von Hertzen[a]

[a] *Department of Applied Mechanics, School of Engineering, Aalto University, FI-00076 Aalto, Finland*

Abstract

As a result of increased speeds, the dynamic instability of rotatory machines including polymer-covered nipped rolls has grown. The instability originates from the viscoelastic behavior of the covers and leads to strong barring vibrations, which limit the operating speed of many machines. In this work, the self-excited vibrations of a nipped two-roll system with a polymer cover on the other roll are investigated using an analytical model developed for the roll system. The viscoelastic properties of the cover are accounted for by the Standard Linear Solid model (SLS). The numerical results display wave-like roll cover deformation patterns, separate instability regions of the system and moving wave patterns near the resonances. The roll system is unstable when the excitation frequency of the polygonal cover deformation lies in the vicinity of the higher eigenfrequency of the system. By using a speed-up ramp, it is shown that at high speeds the instability regions may become too wide and unstable to be crossed in industrial machines. An experiment was carried out, and a good agreement is found between the numerical and experimental results.

Keywords: roll system, polymer cover, Maxwell element, time-delayed feedback, self-excited vibrations, polygonal deformation

1. Introduction

Many industrial applications include cylindrical rolls which rotate in contact with one another. In the nip, that is, within the contact area between the two rolls, the peripheral surfaces of the rolls deform to an out-of-round shape mainly elastically, but possibly also viscoelastically and plastically, depending on the surface materials and loading conditions. In addition, the deformations are significantly influenced by different environmental factors, for example, by temperature and moisture. Removal of the surface material may also occur in the form of wear, grinding and cutting.

The surface deformations recover, for the most part, quite rapidly outside the nip, but what remains after one revolution period is fed back into the nip. The time-delayed feedback causes self-excited vibration in the roll system; this can lead to the formation of a periodic polygonal deformation pattern on the surface of a roll. Furthermore, the wave-like surface pattern may grow gradually, which can be observed as severe, unstable vibration of the rotatory system during its operation. Ultimately, such unstable vibration results in defective products in numerous industrial processes and makes the continuous operation of production machines impossible. Some examples of systems which suffer from these vibrations are the calender and the press rolls of a paper machine, and the winder of a textile machine. In the industrial world, the unstable vibration caused by the deformation pattern, which presents itself to the eye as stripes or bars in the longitudinal (cross-machine) direction of a covered roll, is often referred to as *barring vibration*. The aim of this study is to investigate unstable vibrations in a two-roll system in which the polymer cover and its viscoelastic memory are the source of the vibrations.

[†] **Recompiled, unedited accepted manuscript**. **Cite as**: *J. Sound Vib.* 2011;330(16):3959–3972. doi link

[*] Corresponding author.
Email addresses: anssi.karttunen@aalto.fi (Anssi T. Karttunen), raimo.von.hertzen@aalto.fi (Raimo von Hertzen)

The self-excited vibrations of nipped rolls with time-delayed feedback loads have been a subject of considerable interest recently. Sueoka *et al.* have investigated the pattern formation phenomenon of a polymer cover in a two-roll system both experimentally and theoretically [1]. They have included the viscoelastic properties of the polymer in their analytical lumped-mass model by a three-parameter element possessing one time constant to describe the relaxation process of the polymer. Their computational and experimental results are in close agreement. A similar modeling approach has been used by Sueoka *et al.* in [2]. Moreover, Sowa *et al.* have also used the same type of models to provide a design method to prevent the pattern formation and unstable vibrations in roll systems with polymer covers [3]. Jorkama and von Hertzen have modified the model of Ref. [1] and applied it to the process of paper winding [4, 5]. In these winding configurations, a wound paper roll with an increasing diameter acts as the viscoelastic component of the system. Several fundamental vibration phenomena appearing in real industrial paper winding machines can be identified from their computational results.

Delayed roll systems with viscoelastic memory and grinding effects have also been studied comprehensively by Yuan [6]. Järvenpää and Yuan have extended the study of polymer cover induced roll vibrations by new approaches which include the use of multibody dynamics and finite element method [7], and a contact mechanical model [8]. They have also performed simulations in which an active damping apparatus has been applied to various parts of a nipped roll system to eliminate harmful vibrations [9]. Hermanski has studied the pattern-formation-related vibrations of a paper calender by time domain simulations [10].

Lately, dynamic absorbers have been studied and utilized to eliminate the self-excited vibrations caused by the time-delayed feedback loads. Karhunen has created a functional solution in an experimental study to prevent the unstable vibrations of covered nipped rolls by applying a semi-active dynamic mass absorber to the roll system [11]. Matzusaki *et al.* have investigated self-excited vibrations caused by the surface wear of a steel roll in a steel making machine [12, 13], and Ryu *et al.* have worked on the dynamic instability of a thin sheet winder [14]. The undesired vibrations have been diminished successfully in both applications by using dynamic absorbers.

Extensive experimental studies concentrating on the mechanical behavior of polymer covers in rolling contact and the effect of environmental factors therein have been conducted by Vuoristo *et al.* [15–19]. They have used short duration force pulses to simulate the actual nip loading, which is usually between $0.2 - 1.0$ ms. In addition, they have shown that the temperature and moisture conditions in the nip may affect the deformation behavior of a polymer considerably. Experiments in which the loading is repeated multiple times with short time intervals to simulate real industrial machines are still needed. Valuable experimental data on nipped roll systems have also been given by Chinn [20] and Rautiainen *et al.* [21].

Despite all earlier studies, the polymer cover induced vibrations of nipped rolls are still a problem and the generation mechanism of the self-excited vibrations is not yet fully understood. The development of definitive passive damping and stabilizing methods has been hindered by the lack of physically accurate mathematical models for nipped roll systems. In this paper, to create a basis for more accurate models, a more realistic lumped-mass model is developed for a two-roll system to study the formation of polygonal deformation patterns on a polymer covered roll, and the self-excited vibrations of the system which originate from the deformations. The viscoelastic properties of the cover will be described using the Standard Linear Solid model (SLS) and the model is provided with a possibility of taking into account the complete deformation history of the polymer cover. The stability of the system is investigated numerically and the threshold polygonal number, below which the system becomes unstable, is determined. The polygonal deformation patterns of the cover are considered and the resonance condition of the system is elucidated. The eigenfrequencies of the roll system are also discussed to clarify the effect of the polymer cover properties on the eigenfrequencies, which is often overlooked. By performing an eigenmode analysis, the generation of the self-excited vibration mechanism will be elucidated on the basis of phase-angle relations between the degrees of freedom of the system. Numerical integration of the equations of motion is also performed to demonstrate the effect of acceleration and deceleration ramps on the response of the system. Finally, the numerical results are compared with experimental results gained from a machine corresponding to the presented model.

2. Theory

Let us consider the system shown in Fig. 1. The system consists of two rolls and a polymer cover. The rolls are modeled by masses m and M. The SLS polymer cover of the upper roll is massless. The vertical displacement coordinates for the upper and lower roll are x and X, respectively. The roll supports are modeled by springs and viscous dashpots with stiffness and viscous damping coefficients k and c for the upper roll, and K and C for the lower roll, respectively. The parameters for the SLS element are k_∞, k_1 and c_1, where the latter two form a Maxwell element. The coordinate z determines the movement of the spring's end plate in the damper of the Maxwell element.

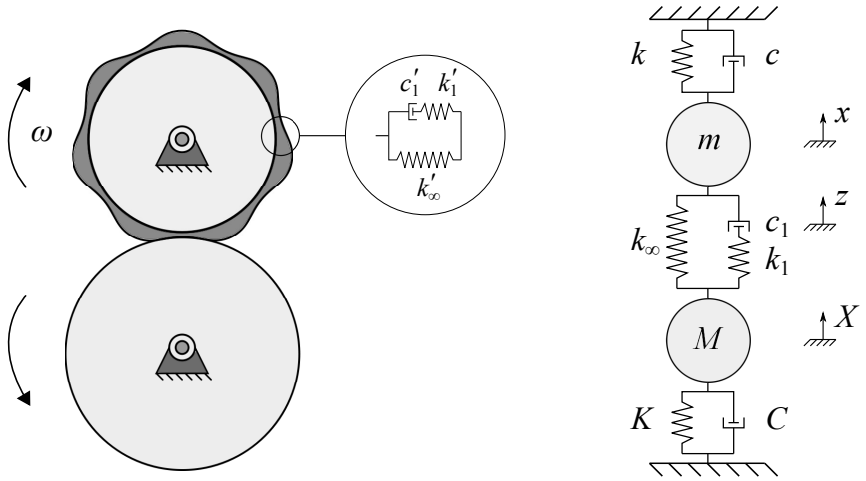

Figure 1: Two-roll system with a polymer cover attached to the upper roll. A deformed polygonal shape of the cover is shown. In the one-dimensional model the rolls are modeled as rigid bodies and the cover by an SLS element.

2.1. Formulation of the feedback deformations

In the present model, only the nip force affects the deformation of the polymer cover; no environmental factors have been accounted for. The extensional viscous deformation of the polymer cover is defined by

$$\Delta l(t) = x(t) - z(t) \ . \tag{1}$$

When the SLS element of Fig. 1, attached to the upper roll and rotating with it, is located outside the nip, the force equilibrium of the element gives (here x and z refer to the rotated configuration)

$$\begin{cases} k_\infty x + c_1 \left(\dot{x} - \dot{z}\right) = 0 \\ k_1 z - c_1 \left(\dot{x} - \dot{z}\right) = 0 \end{cases} \ , \tag{2}$$

from which one obtains for the viscous deformation of the element outside the nip

$$\Delta l(t) = e^{A(t-t_0)} \Delta l(t_0) \ , \tag{3}$$

where $\Delta l(t_0)$ is the viscous deformation of the element at time t_0 when the element comes out of the nip. The recovery coefficient of the deformation is

$$A = -\frac{k_\infty}{k_\infty + k_1} \ \frac{1}{\tau_1} \ , \tag{4}$$

where $\tau_1 = c_1/k_1$ is the relaxation time of the polymer cover. When the element enters the nip after one revolution at time t, it contains a non-recovered viscous residual deformation

$$\Delta l(t^-) = e^{AT_1} \left[x(t - T_1) - z(t - T_1) \right] \ , \tag{5}$$

where T_1 is the length of the previous revolution period of the upper roll. In the nip, the new viscous deformation is added to the residue from the previous period, thus the total deformation when the element leaves the nip can be divided into two parts

$$\Delta l(t^+) = \underbrace{x(t) - z(t)}_{\text{current period}} + \underbrace{\Delta l(t^-)}_{\text{previous period}} \quad . \tag{6}$$

By generalizing this superposition principle, it can be seen that when the SLS element enters the nip, the total non-recovered viscous deformation is the sum of all contributions from preceding periods, that is,

$$\Delta l(t^-) = \sum_{k=1}^{N} e^{AT_k} \left[x(t - T_k) - z(t - T_k) \right] \ , \tag{7}$$

where N is the number of complete revolution periods of the upper roll at time t and T_k is the time spent for k preceding periods. In conclusion, the use of the sum in Eq. (7) is a consequence of the one-dimensionality of the model and bears close resemblance to the Boltzmann superposition principle [22].

2.2. Equations of motion of the system

The equations of motion for the two rolls and the cover can be shown to be of the form

$$\mathbf{M}\ddot{\mathbf{X}}(t) + \mathbf{C}\dot{\mathbf{X}}(t) + \mathbf{K}\mathbf{X}(t) = \mathbf{K}_1 \sum_{k=1}^{N} e^{AT_k} \mathbf{X}(t - T_k) \ , \tag{8}$$

for which the explicit expression is

$$\begin{bmatrix} m & 0 & 0 \\ 0 & 0 & 0 \\ 0 & 0 & M \end{bmatrix} \begin{Bmatrix} \ddot{x} \\ \ddot{z} \\ \ddot{X} \end{Bmatrix} + \begin{bmatrix} c + c_1 & -c_1 & 0 \\ -c_1 & c_1 & 0 \\ 0 & 0 & C \end{bmatrix} \begin{Bmatrix} \dot{x} \\ \dot{z} \\ \dot{X} \end{Bmatrix} + \begin{bmatrix} k + k_\infty & 0 & -k_\infty \\ 0 & k_1 & -k_1 \\ -k_\infty & -k_1 & k_1 + k_\infty + K \end{bmatrix} \begin{Bmatrix} x \\ z \\ X \end{Bmatrix}$$
$$= k_1 \begin{bmatrix} 1 & -1 & 0 \\ 0 & 0 & 0 \\ -1 & 1 & 0 \end{bmatrix} \sum_{k=1}^{N} e^{AT_k} \begin{Bmatrix} x(t - T_k) \\ z(t - T_k) \\ 0 \end{Bmatrix} \ . \tag{9}$$

The driving force due to residual deformation is exerted on both rolls in the nip as an impact via the spring of the Maxwell element, the damper being momentarily stiff due to the lack of time to react under the load of the residual deformation entering the point-like nip (see Eq. (7) and the right hand side of Eq. (9)). If the revolution frequencies of the rolls are constant, the period of the upper roll is a constant T, implying that $T_k = kT$.

In this work, the primary aim is to study the stability loss and small amplitude vibrations of the system. It is well-known that a non-conformal contact and the cover material itself exhibit non-linear behavior in stiffness and damping at larger vibration amplitudes [20, 23]. However, the main emphasis in the study of barring vibrations lies in the stability loss and small amplitude vibrations, which are enough to create severe problems in industrial machines. The large amplitude limit cycles, or the way how the cover breaks down, are not of notable interest. Therefore, the model is limited here to a linear one. This argument also applies to more advanced models accounting for corrective measures against barring vibrations, such as dynamic mass absorbers or active control systems.

2.3. Stability analysis and complex eigenmodes

If the rolls rotate at constant speeds, the stability of the system can be investigated by Laplace transforming Eq. (9) from the time domain t to the Laplace domain s. When the initial conditions are set to zero, the Laplace transform of Eq. (9) can be written as

$$\begin{bmatrix} ms^2 + (c + c_1)s + k + k_\infty - k_1\alpha & -c_1 s + k_1\alpha & -k_\infty \\ -c_1 s & c_1 s + k_1 & -k_1 \\ -k_\infty + k_1\alpha & -k_1(1 + \alpha) & Ms^2 + Cs + k_1 + k_\infty + K \end{bmatrix} \begin{Bmatrix} \hat{x} \\ \hat{z} \\ \hat{X} \end{Bmatrix} = 0, \tag{10}$$

where the delay parameter α is

$$\alpha = \sum_{k=1}^{N} e^{kAT} e^{-ksT} \ . \tag{11}$$

The characteristic equation of the system is

$$\det \mathbf{A} = 0 \ , \tag{12}$$

where $\mathbf{A}$ is the multiplication matrix of Eq. (10). The complex valued roots $s_i = \alpha_i + j\beta_i$ can be solved from Eq. (12). The system is stable if the real parts of all roots are negative. On the other hand, the system is unstable if even one of the real parts is positive. The long-term behavior of the roll system can be predicted on the basis of the roots. The higher the value of the real part of a root is, the faster the surface deformations of the polymer cover and the self-excited vibrations of the system grow. The characteristic equation has an infinite number of roots, because of the complex transcendental exponential function in Eq. (11). The imaginary part of each root can be written in the form

$$\mathrm{Im}[s_i] = 2\pi N_i f \ , \tag{13}$$

where f is the revolution frequency of the upper roll and N_i is the so called *polygonal number*. The polygonal number gives essential information on the deformation pattern of the polymer cover. The pattern is evidently linked to the vibration frequency of the system – the shape of the pattern is determined by the number of vibration periods of the upper roll in one revolution period T. Although the system has an infinite number of the described *polygonal roots*, the study can be limited to those roots, which correspond to the actual deformation patterns appearing in real industrial machines.

By substituting the solved polygonal roots back to Eq. (10), the complex eigenmodes of the roll system corresponding to each polygonal root can be calculated. The (relative) vibration amplitudes and phase angles for the degrees of freedom can be solved from the complex eigenmodes by the equations

$$\left|\hat{\mathcal{X}}_i\right| = \sqrt{\mathrm{Re}[\hat{\mathcal{X}}_i]^2 + \mathrm{Im}[\hat{\mathcal{X}}_i]^2} \ , \tag{14}$$

$$\arg(\hat{\mathcal{X}}_i) = \arctan \frac{\mathrm{Im}[\hat{\mathcal{X}}_i]}{\mathrm{Re}[\hat{\mathcal{X}}_i]} \ , \tag{15}$$

where $\hat{\mathcal{X}}_i = \hat{x}_i, \hat{z}_i, \hat{X}_i$. It is possible to generate eigensolutions for the system of the form

$$\begin{Bmatrix} x \\ z \\ X \end{Bmatrix}_i (t) \ = \begin{Bmatrix} \hat{x} \\ \hat{z} \\ \hat{X} \end{Bmatrix}_i e^{s_i t} \qquad \text{or} \qquad \mathbf{X}_i(t) = \hat{\mathbf{X}}_i e^{s_i t} \ , \tag{16}$$

where s_i is a complex valued root of the characteristic equation and $\hat{\mathbf{X}}_i$ is the corresponding complex eigenmode. Based on the Maxwell element's force equilibrium, the relation

$$(\hat{x} - \hat{z})_i = \frac{1}{\sqrt{(1+\alpha_i\tau_1)^2 + \beta_i^2\tau_1^2}} (\hat{x} - \hat{X})_i \, e^{-j\phi_i} \tag{17}$$

for the ith eigenmode can now be written between the viscous deformation $(\hat{x}-\hat{z})_i$ and the nip gap $(\hat{x}-\hat{X})_i$. The phase shift ϕ_i between these two can be calculated from

$$\tan\phi_i = \frac{\beta_i\tau_1}{1+\alpha_i\tau_1} \qquad (0 \le \phi_i < \pi/2). \tag{18}$$

It can also be easily shown that, for the ith eigenmode, the phasor of the residual deformation Δl is

$$\Delta\hat{l}_i = \sum_{k=1}^{N} e^{kAT} e^{-ks_iT} (\hat{x} - \hat{z})_i \ . \tag{19}$$

Therefore, the amplitude and phase angle of the residual deformation can also be calculated. The relations (18) and (19) will be used later.

2.4. Modal damping coefficients and eigenfrequencies of the system

By removing the viscous memory effect from the system or by stopping the rotational motion of the rolls, the characteristic equation becomes a polynome, because Eq. (11) must be replaced by $\alpha = 0$. One can calculate the modal damping coefficients and eigenfrequencies of such a system from the roots of this characteristic equation by using the equations [24] (now $i = 1, 2$)

$$\zeta_i = -\frac{\mathrm{Re}[s_i]}{\sqrt{\mathrm{Re}[s_i]^2 + \mathrm{Im}[s_i]^2}} \ , \tag{20}$$

$$f_{n,i} = \frac{\sqrt{\mathrm{Re}[s_i]^2 + \mathrm{Im}[s_i]^2}}{2\pi} \ . \tag{21}$$

Alternatively, the undamped (angular) eigenfrequencies can be calculated by using the equation

$$\det\left(\begin{bmatrix} k + k_\infty + k_1 & -k_\infty - k_1 \\ -k_\infty - k_1 & K + k_1 + k_\infty \end{bmatrix} - \omega_n^2 \begin{bmatrix} m & 0 \\ 0 & M \end{bmatrix}\right) = 0 \ , \tag{22}$$

which corresponds to the limit $c_1 \to \infty$. The approach of Eq. (22) is often used in simple analyses.

2.5. Change of variables in the equations of motion

For the numerical analysis, a change of variables is performed in Eq. (8) by changing the time variable t to the revolution angle θ of the upper roll. Let the revolution angle $\theta = \theta(t)$ of the upper roll be a given function. The equation for the revolution angle can be inverted, that is, $t = t(\theta)$. After this the angular speed $\dot{\theta}(t)$ and angular acceleration $\ddot{\theta}(t)$ can be written as functions of the revolution angle, that is, $\omega = \omega(\theta)$ and $\alpha = \alpha(\theta)$. Performing the change of variables from t to θ in Eq. (8) results in

$$\omega^2(\theta)\mathbf{M}\mathbf{X}''(\theta) + \big(\alpha(\theta)\mathbf{M} + \omega(\theta)\mathbf{C}\big)\mathbf{X}'(\theta) + \mathbf{K}\mathbf{X}(\theta) = \mathbf{K}_1 \sum_{k=1}^{N} a_k(\theta)\mathbf{X}(\theta - 2\pi k) \ . \tag{23}$$

Here $a_k(\theta) \equiv e^{AT_k(t(\theta))}$ and $\mathbf{X}(\theta) \equiv \mathbf{X}(t(\theta))$, and the prime stands for differentiation with respect to θ. The quantity $T_k(t(\theta))$ is the time spent for k preceding periods. In the special case when the angular acceleration vanishes, the angular speed $\omega(\theta)$ is constant, and Eq. (23) rearranges as

$$\omega^2\mathbf{M}\mathbf{X}''(\theta) + \omega\mathbf{C}\mathbf{X}'(\theta) + \mathbf{K}\mathbf{X}(\theta) = \mathbf{K}_1 \sum_{k=1}^{N} a_k\mathbf{X}(\theta - 2\pi k) \ , \tag{24}$$

where $a_k = e^{kAT}$ and $T = 2\pi/\omega$. The results, computed as a function of the revolution angle of the upper roll, can be easily transformed back to the time domain. The use of the revolution angle as the non-dependent variable is advantageous, because the delay terms can be formed easily. This is especially true when the system possesses angular acceleration (cf. the right hand sides of Eqs. (23) and (8)).

2.6. Numerical analysis

In this work, the roots of the characteristic equation are solved by using Müller's method [25]. This iterative method is based on the secant method but uses quadratic interpolation instead of linear. In addition, Müller's method requires no derivatives and can accommodate complex valued roots as well, if the given starting values are complex and the computations use complex arithmetic. The computations are performed by using MATLAB 7.7.

For the numerical integration, Eqs. (23) and (24) are transformed into state space presentation. The equations are integrated using MATLAB 7.7 and its ode45 solver. After every integration step the solver calls for its own output function, and the results are transferred therein and saved as vectors. The results can be read from the computer memory during the integration to create the time delay terms for the computations. The procedure is an adaptation of the method of steps [26]. Other ode-solvers may be used

as well. Therefore, if the differential equations are stiff because of the parameters of the system, ode15s can be used. Alternatively, the well-known solvers for delay differential equations, dde23 and ddesd, could be used, but these are not optimized for the studied case and thus lack the speed of ode45 combined with the method of steps. To investigate the results in the frequency domain, the Fast Fourier Transform (FFT) is used.

3. Results and discussion

In the numerical analysis, a simulation case was studied with parameter values acquired from a two-roll industrial testing machine corresponding to the model in Fig. 1. The machine has been built to investigate the dynamic behavior of paper calenders and size presses including a polymer-covered roll. In this study, the upper roll of the machine had a polymer cover, which is utilized in soft calendering applications. The standard values for the calculations are shown in Table 1. The relaxation time of the polymer was set to $\tau_1 = 0.85$ ms. In a more detailed scenario, the recovery of the polymer would be determined by a relaxation spectrum spanning a large scale of relaxation times. This would require the generalization of the SLS model in Fig. 1 by increasing the number of the Maxwell elements. In this type of model, the interaction between the fast and slowly relaxing Maxwell elements would bring its own contribution to the system dynamics. However, it has been shown that a simple viscoelastic element possessing one relaxation time is enough to adequately model the behavior of the viscoelastic roll cover, if the element's recovery outside the nip is retarded [1]. Nevertheless, let us note that the results obtained by such a model are qualitative by nature. In the case of the model presented in this paper, the relaxation coefficient A, Eq. (4), was divided by 350 to account for the slowly relaxing viscous elements and the strain rate dependence of the polymer cover [1]. The dynamic behavior of the system was investigated by taking the viscoelastic memory of the polymer cover into account only from the previous period, thus $N = 1$. A thorough analysis of this elementary case, which nonetheless presents notable complexity as the results will show, creates a necessary basis for future studies. Our numerical studies show that the effect of a more extensive memory on the system dynamics is mainly quantitative, that is, it affects the magnitude of the time-delayed feedback force and slightly lowers the instability threshold of the roll system, but does not change the overall physical behavior of the system in a drastic manner. In all earlier studies which use a corresponding one-dimensional model, the memory has been accounted for only from the previous period and the need for the sum in the residual deformation equations has not been discussed.

Table 1: Standard parameter values of the roll system for the computations.

Parameter	m	c	k	M	C	K	k_∞	k_1	c_1	τ_1
Value	569	8350	51.8	5380	65400	265	615.5	99.28	84.38	0.85
Unit	kg	Ns/m	MN/m	kg	Ns/m	MN/m	MN/m	MN/m	kNs/m	ms

3.1. Modal damping coefficients and eigenfrequencies of the roll system

Given by Eq. (20), the first and second modal damping coefficients of the non-rotating system with the standard parameter values are $\zeta_1 = 0.027$ and $\zeta_2 = 0.043$, respectively. Therefore, the damping of the system is clearly subcritical, as the damping coefficients satisfy the condition $\zeta_i < 1$. When calculated from Eq. (21), the eigenfrequencies of the system are $f_{n,1} = 36.68$ Hz and $f_{n,2} = 187.3$ Hz. The corresponding values calculated from Eq. (22) are 36.69 Hz and 193.4 Hz.

Fig. 2 shows how the values of the higher eigenfrequency $f_{n,2}$ and the modal damping coefficient ζ_2 calculated from Eqs. (21) and (20), respectively, change when the relaxation time $\tau_1 = c_1/k_1$ is altered by changing the value of c_1. The eigenfrequency calculated from Eq. (22) with the standard value of k_1 and with $k_1 = 0$ is depicted by the upper and lower dotted lines, respectively. It can be seen that the eigenfrequency has a transition zone within which its value is highly dependent on the relaxation time. For

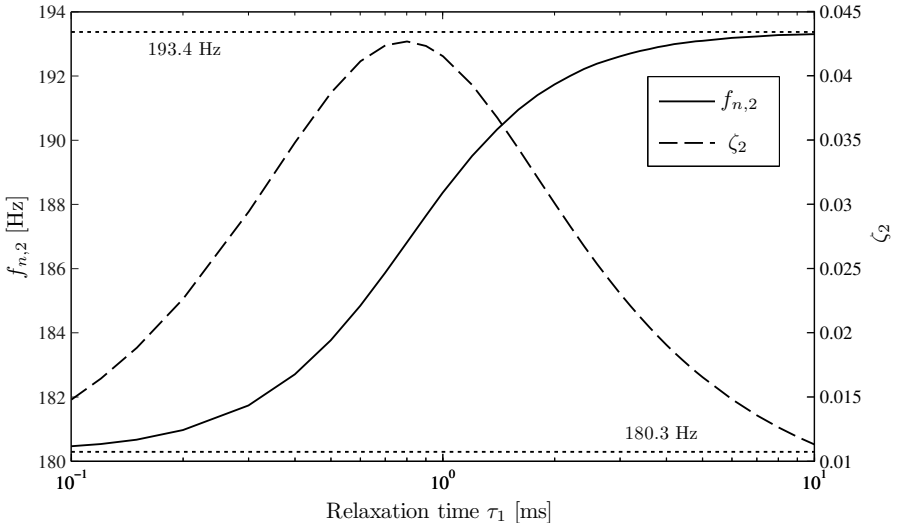

Figure 2: Effect of the relaxation time of the Maxwell element on the eigenfrequency $f_{n,2}$ and the modal damping coefficient ζ_2 of the system. The eigenfrequency has a specific transition zone within which its value depends significantly on the value of the damping coefficient c_1 of the Maxwell element. Near the lower boundary (180.3 Hz) the Maxwell element damper acts loosely, and as the relaxation time grows, it becomes stiffer. For the standard value of c_1, the value $f_{n,2} = 187.3$ Hz is obtained.

short relaxation times, the spring of the Maxwell element can be pictured as moving in the damper without notable resistance. Correspondingly, for high values of τ_1 the viscosity of the damper is high, making the Maxwell element stiff, so that the eigenfrequency $f_{n,2}$ given by Eq. (21) approaches the value 193.4 Hz of the upper dotted line. The modal damping coefficient reaches its peak value when the change of the eigenfrequency from the lower to the upper boundary is approximately midway (186.8 Hz). At this point, the Maxwell element dissipates energy at the maximum rate. Note the large alteration of the modal damping coefficient between approximately $1 - 4$ % within the transition zone.

3.2. Numerical stability analysis

In the first eigenmode of the system the rolls are vibrating practically in the same phase. In this case, it is difficult for the deformation pattern of the roll cover to take a polygonal form. Therefore, self-excited unstable vibration does not emerge. In the second eigenmode the rolls are vibrating almost in opposite phases, colliding strongly with each other, and causing roll cover deformations which are able to synchronize with the second eigenmode. As the deformations of the cover develop in time, the vibration amplitudes of the rolls grow exponentially and lead to self-excited unstable vibrations.

Fig. 3 shows the polygonal numbers $N_1, N_2, ..., N_{15}$ of the characteristic roots $s_1, s_2, ..., s_{15}$ as a function of the revolution frequency f of the upper roll. The roots have been calculated from Eq. (12) using the standard parameter values, and the polygonal numbers from Eq. (13). The subscript notation $i = 1, 2, \ldots, 15$ refers to the polygonal number (rounded to the nearest integer) of the corresponding root at the revolution frequency $f = 1$ Hz of the upper roll. In addition, the unstable parts of the complex roots ($\alpha_i > 0$) are illustrated by thicker lines in the figure, and the eigenfrequencies computed from Eq. (21) have been presented relative to the revolution frequency, that is, $\hat{f}_1 = f_{n,1}/f$ and $\hat{f}_2 = f_{n,2}/f$.

It can be seen from Fig. 3 that the instability of the system arises when the frequency of the deformation pattern (polygonal shape) induced excitation is equal or almost equal to the higher eigenfrequency of the system, i.e., $fN_i \approx f_{n,2}$. Therefore, the unstable vibration of the system is related to the resonance vibration. As a result, the unstable vibrations appear only in certain revolution frequency areas; these areas widen as the revolution frequency grows. Correspondingly, at lower frequencies, the unstable areas vanish completely. The system has a clear instability threshold related to the root s_{12} at the revolution frequency $f = 15.8$ Hz.

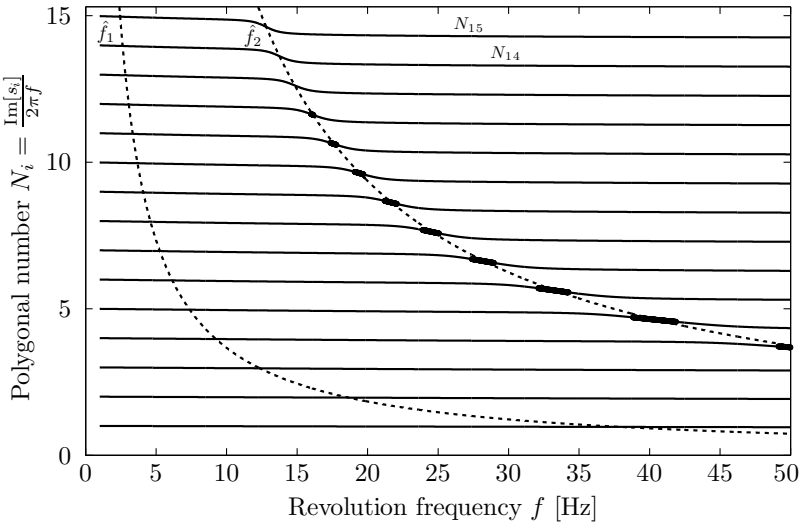

Figure 3: Polygonal numbers as a function of the revolution frequency of the upper roll. The thicker lines represent the unstable areas of the roll system. There is an instability threshold at $f = 15.8$ Hz.

All the polygonal numbers behave qualitatively in the same manner in Fig. 3. For a closer look, a magnification of N_{10} and N_9 is presented in Fig. 4. At low revolution frequencies, the polygonal numbers of the roots are close to an integer, that is, the cover deformation pattern of a slowly rotating system is a full wave-like formation on the peripheral surface of the roll.

When the polygonal numbers are in the influence area of curve $\hat{f}_1$ related to the lower eigenfrequency, a small increase can be seen in their values; nevertheless, the roots stay stable. After they have passed curve $\hat{f}_1$ and approach curve $\hat{f}_2$ related to the higher eigenfrequency, their values continue to decrease steadily. The decreasing non-integer polygonal number is related to the fact that, when observed from the side, it seems as if the surface pattern was moving in the opposite direction relative to the roll's rotational motion. This motion has been discussed also in Ref. [1] on the basis of experimental and numerical results. A drastic fall can be observed in the polygonal numbers in the vicinity of curve $\hat{f}_2$. Due to the resonance of the second eigenmode, the system also becomes unstable. After the resonance, the polygonal numbers of the roots exhibit a steady decrease again, approaching asymptotically a constant value as the revolution frequency grows. From the figure, one can calculate that when N_{10} (N_9) crosses curve $\hat{f}_2$, the frequency of the deformation pattern induced excitation is 19.4 Hz $*$ 9.63 $\approx$ 187 Hz (21.7 Hz $*$ 8.63 $\approx$ 187 Hz). This should be compared to the eigenfrequency $f_{n,2} = 187.3$ Hz of the non-rotating system.

The real parts of several polygonal roots are shown in Fig. 5. At the revolution frequency $f = 1$ Hz, the value of each real part is very close to -5. No significant changes can be seen in the vicinity of curve $\hat{f}_1$ (see Fig. 3). The real parts are near their maximum positive values when the corresponding polygonal numbers of the roots cross curve $\hat{f}_2$. It has been verified by several authors that the unstable and stable regions alter as the revolution frequency (speed) of the covered roll changes. Refs. [1–3, 7, 8, 14] show such computational results with various models. Even though the general solution of the system is the sum of solutions formed from Eq. (16), the general behavior of the roll system in the unstable areas can be investigated satisfactorily on the basis of individual roots, since only one root is unstable at a time.

The effect of increased roll support damping can be observed in Fig. 6. The real parts of four roots have been calculated using the standard values of c and C, and their values multiplied by a factor of 2. The increase in damping lowers the values of the real parts stabilizing the system. However, it is important to note that the model does not account for the bending vibrations of the rolls. In a case in which the roll supports are relatively stiff, the elimination of the unstable vibrations in the middle of the rolls can be especially hard by only increasing the damping in the roll supports. Let us conclude that, in any case, the

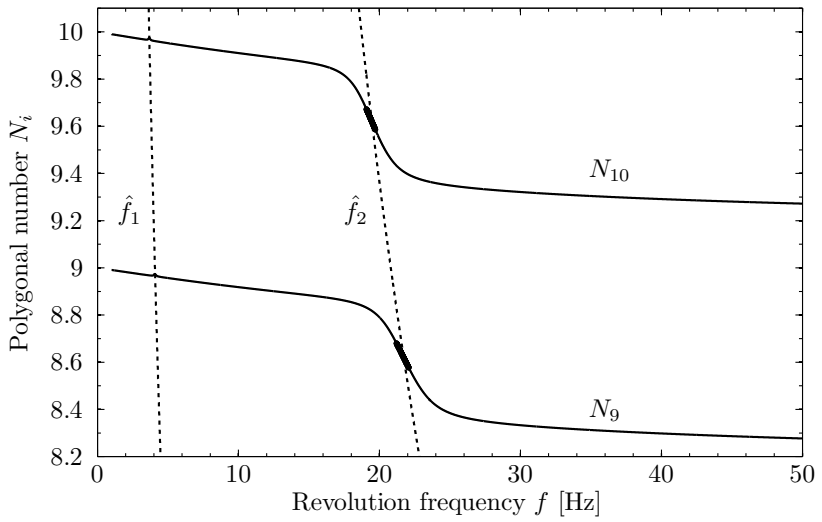

Figure 4: Polygonal numbers N_{10} and N_9 as a function of the revolution frequency of the upper roll. The deviation from integer values is related to the movement of the deformation pattern of the polymer cover. The thicker lines represent the unstable areas.

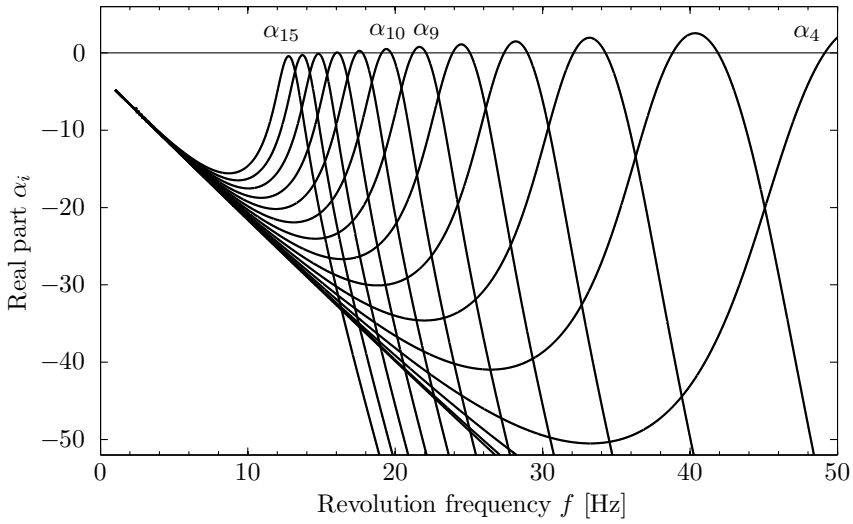

Figure 5: Real parts of polygonal roots. Only one root is unstable at a time. Each real part reaches its maximum value at the same revolution frequency as the root's polygonal number crosses the curve $\hat{f}_2$ corresponding to the higher eigenfrequency in Fig. 3.

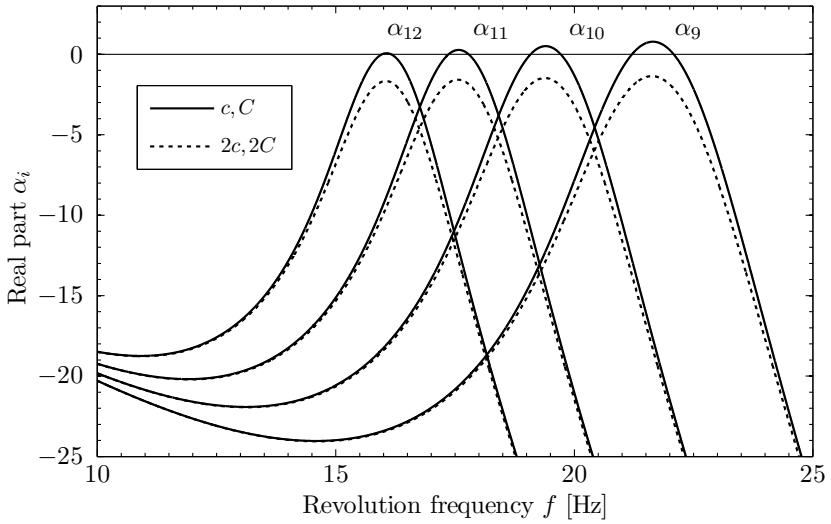

Figure 6: Effect of increased roll support damping on the stability of the system. Doubling of the support damping renders the originally unstable roots $s_{12}, s_{11}, \ldots, s_4$ stable (only four real parts are shown).

design of proper damping is a question of optimization between stiffness and damping.

By calculating the complex eigenmodes of the system from Eq. (10) by back-substitution for the root s_{10}, the phase angles of the system corresponding to the root s_{10} can be studied. Fig. 7 shows various phase-angle relations between the degrees of freedom of the roll system as a function of the revolution frequency of the upper roll. The polygonal root s_{10} is unstable between $f = 19.1 - 19.7$ Hz and dominates the behavior of the roll system only in this area. If the eigenmode corresponding to s_{10} arises outside the unstable area, it fades out quickly. Nevertheless, the presentation of Fig. 7 is particularly useful in gaining information on the polymer cover's deformation mechanism, which causes the dynamic instability of the roll system.

It can be seen from the phase shift $\arg(\hat{x}) - \arg(\hat{X})$ between the rolls that the polygonal shape of the cover corresponding to the polygonal number N_{10} keeps the system almost invariably in the higher eigenmode, in which the rolls are in opposite phases. In the vicinity of the lower eigenfrequency (see curve $\hat{f}_1$ in Fig. 3) the rolls, however, strive for the lower eigenmode. The phase shift decreases almost to zero, so the rolls are nearly in the same phase.

The phase shift between the nip gap and the viscous deformation of the cover $\arg(\hat{x} - \hat{X}) - \arg(\hat{x} - \hat{z})$ indicates that, at low revolution frequencies, the viscous deformation and the nip gap are nearly in the same phase. As the revolution frequency grows, so does the phase shift. The phase shift is 45 degrees when the instability peak at $f = 19.4$ Hz is met; if the phase shift is calculated directly from Eq. (18), the result is the same. At high revolution frequencies, the phase shift approaches 90 degrees. Near the unstable region, the phase angle $\arg(\Delta\hat{l})$ of the residual deformation has a peculiar transition zone. When the real part of the root s_{10} is at its maximum ($f = 19.4$ Hz), the phase of the residual deformation precedes the nip gap by 90 degrees. Based on this, it can be deduced that the maximum (minimum) of the residual deformation, i.e, the hill top (valley) of the deformation pattern, enters the nip at an instance at which the rolls are in their equilibrium positions and their velocities are at peak values. If the rolls are separating from each other, an elevated part on the polymer cover enters the nip to amplify the vibration. Correspondingly, if the rolls are moving towards each other, a sunken part of the cover enters the nip. In conclusion, the phase shifts are favorable for the growth of the self-excited vibrations, and the situation corresponds to the resonance of a 1-DOF system, where the driving force precedes the displacement by 90 degrees. Furthermore, it can be seen that no such situation appears concerning the lower eigenfrequency of the system. Beyond the unstable region, the phase shift between the residual deformation and the nip gap settles at 180 degrees.

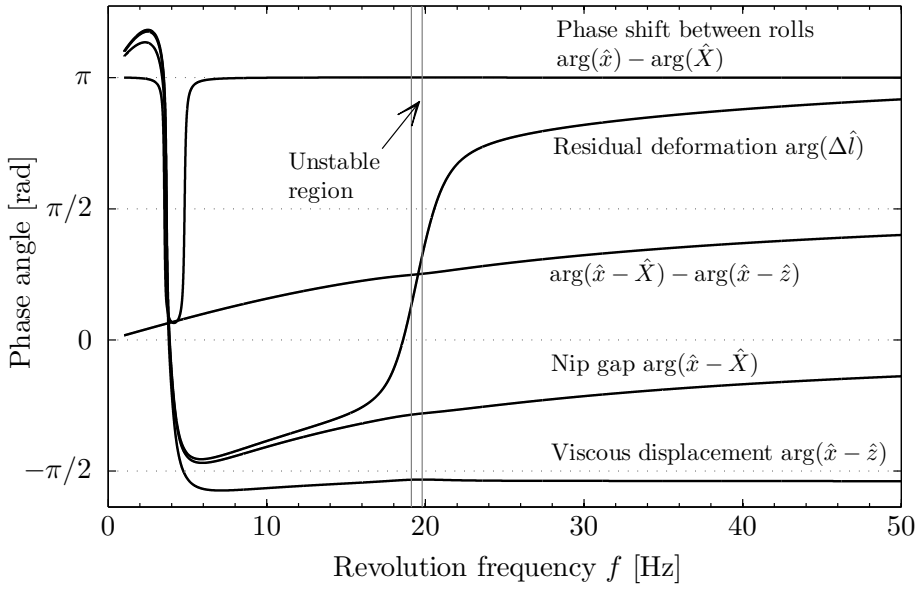

Figure 7: Phase-angle relations of the system's eigenmode corresponding to the root s_{10} calculated from Eq. (15). In the calculations, the value $\hat{z} = 1$ was used. The polygonal shape of the cover keeps the rolls almost invariably in the higher eigenmode. When the real part of s_{10} reaches its maximum value, the phase shift between the residual deformation and the nip gap is 90 degrees.

3.3. Integration of the equations of motion

Displacement responses of the rolls integrated from Eqs. (24) with a constant revolution frequency $f = 19.4$ Hz of the upper roll are shown in Fig. 8(a). The initial condition for the lower roll's displacement was $X(0) = -0.001$ m, with all other displacements and velocities set to zero. FFT was performed on the data of the upper roll and Fig. 8(b) shows the acquired power spectrum (DFT-amplitude^2/transform length), which represents the contribution of every frequency of the spectrum to the power of the overall signal.

Fig. 8(a) indicates that the system is unstable at the revolution frequency in question. The vibration amplitudes of the rolls grow exponentially. The small window shows the steady-state response of the system during one revolution period. It can be seen that the rolls are in opposite phases. In the power spectrum of the signal in Fig. 8(b), the peak value appears at the frequency 187 Hz, which corresponds to the higher eigenfrequency of the system. By dividing the peak frequency by the revolution frequency, we get 187 Hz / 19.4 Hz = 9.6. This is the polygonal number (wave-number) of the wave-like deformation pattern of the covered roll (cf. with Fig. 4). The results of Figs. 8(a) and 8(b) correspond to those of the stability analysis: the unstable root s_{10} is dominant.

Fig. 9 shows an integration result calculated from Eqs. (23) using different values for the angular acceleration of the upper roll to model a speed-up/down ramp. The upper part of the figure shows the responses of the rolls and the lower part the revolution frequency of the upper roll, all as a function of the upper roll's revolution angle. The speeding up starts at $f = 17$ Hz. The revolution frequency is raised using a linear ramp having a constant angular acceleration of 1.0 rad/s^2. At the end of this acceleration stage, the upper roll rotates at $f = 22$ Hz. At this frequency, the root s_9 is unstable in the stability analysis. Then, the revolution frequency is lowered to 21 Hz by using a linear ramp with an angular acceleration of -1.0 rad/s^2. In the areas of influence of the polygonal numbers N_{11}, N_{10} ja N_9, the self-excited vibrations caused by the emerging cover deformations raise the vibration amplitudes. When accelerating real industrial machines to certain speeds, the unstable regions might cause problems. At some point, the instability regions may become too wide and unstable to be crossed.

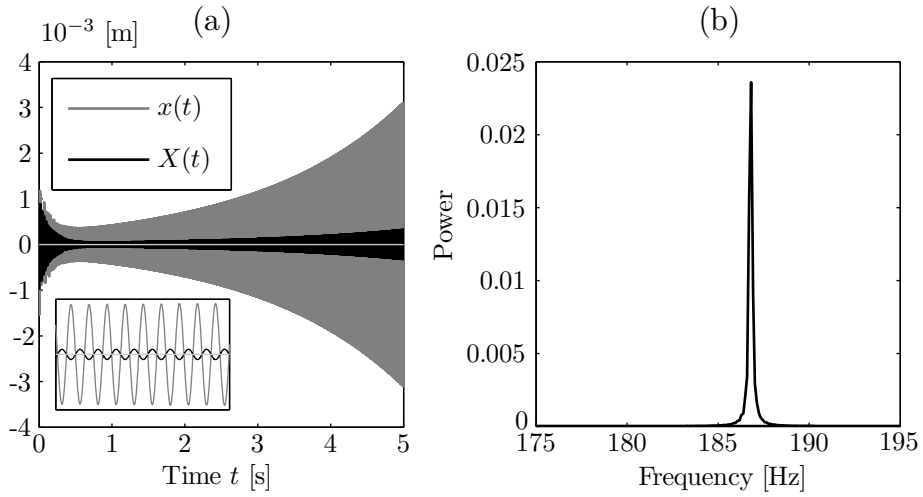

Figure 8: (a) Displacement responses of the rolls integrated from Eqs. (24) with a constant revolution frequency of 19.4 Hz. The system is unstable and in resonance because of the self-excited vibrations caused by the polymer cover. In the small window the displacements during one revolution period around $t = 4$ s are shown. (b) Power of the upper roll calculated by FFT using the time interval 0 – 5 s presented in Fig. 8(a). The peak value appears at 187 Hz.

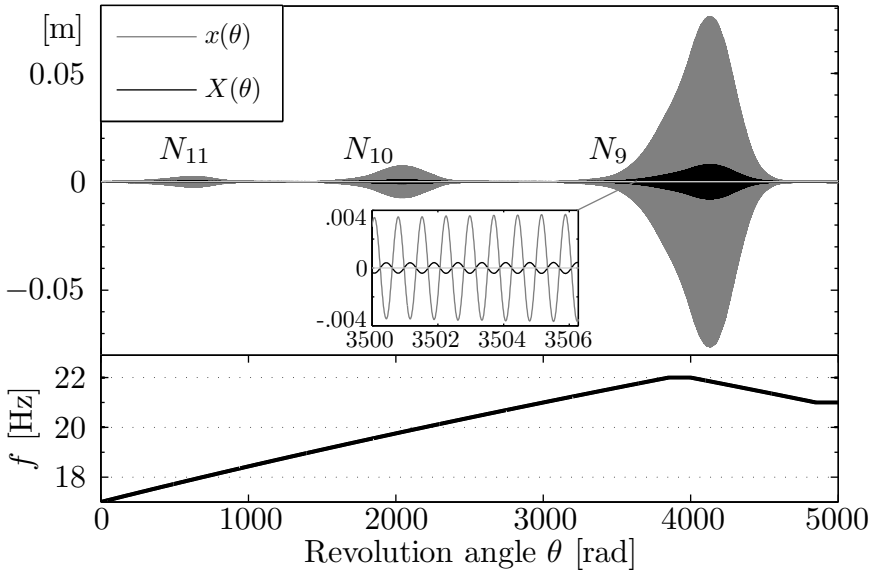

Figure 9: Displacement responses of the rolls with a changing revolution frequency of the upper roll. The values used for the angular acceleration are 1 rad/s^2, 0, –1 rad/s^2 and 0 (from the beginning). The vibration amplitudes of the rolls grow in the unstable areas.

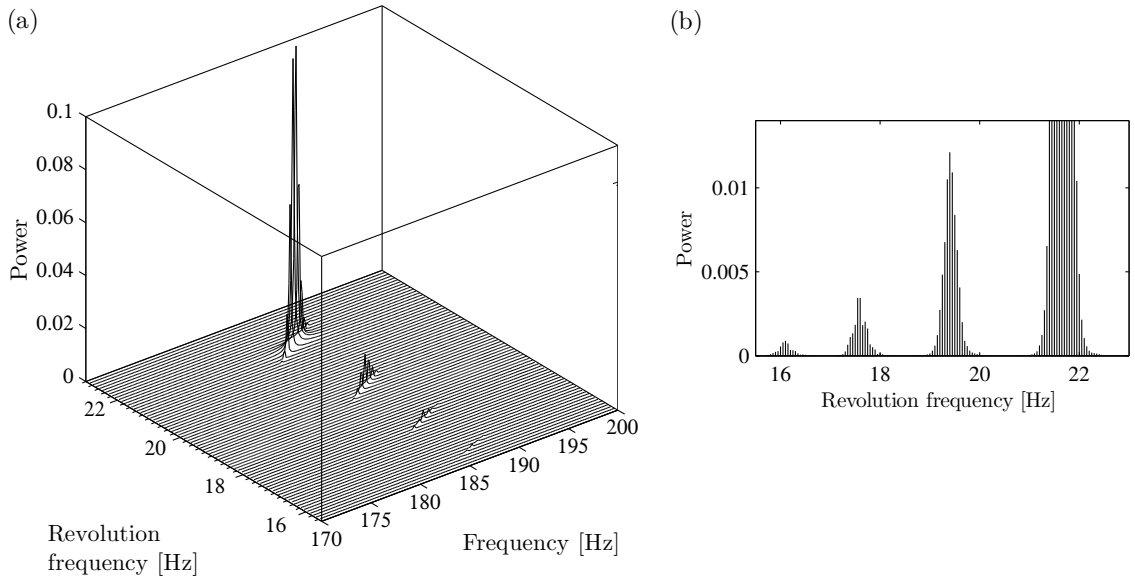

Figure 10: (a) Cascade plot formed from separate power spectra. (b) Power-revolution frequency perspective of the same plot. The unstable vibration appears clearly in the vicinity of the higher eigenfrequency of the system ($f_{n,2} = 187.3$ Hz). The vibration levels grow severely as the revolution frequency of the upper roll grows.

Figs. 10(a) and 10(b) show a cascade plot combined from separate power spectra, which have been calculated in the same way as in Fig. 8(b). The figures clearly indicate the separate unstable regions of the system. The unstable vibrations appear mainly in the frequency zone $185 - 189$ Hz. The results shown in Figs. 9 and 10 are in good concordance with measured data from actual machines [1, 6].

4. Comparison with experimental results

In order to get empirical information on the polymer cover induced self-excited vibrations in a rolling contact system, an experiment was carried out using the same machine which was previously modelled and studied numerically. In the following section, the polymer cover deformations and the related self-excited vibrations are referred to as barring for the sake of brevity.

The maximum rotational speed of the polymer-covered upper roll of the machine was 1500 rpm ($f = 25$ Hz). Only the upper roll was rotated by a motor while the lower roll rotated due to frictional forces in the nip. In the experiment, the nip was formed and the upper roll was accelerated to 1500 rpm in 15 minutes. From 1500 rpm, the speed was lowered quickly to 1400 rpm. Based on the numerical calculations, the polygonal number N_9 should cause instability in the system between $1326 \ldots 1272$ rpm ($22.1 \ldots 21.2$ Hz). The main purpose of the test was to drive slowly through this zone starting from 1400 rpm and investigate the occurring phenomena. Between $1400 \ldots 1330$ rpm the system remained stable, after which the vibration level began to rise rapidly in an exponential fashion. Fully-developed barring can be examined in Fig. 11. Fig. 11(a) shows the rotational speed of the upper roll and its vibration signal, i.e., the measured root-mean-square vertical acceleration. Fig. 11(b) shows the real-time power spectrum calculated from the vibration signal between $1310 \ldots 1270$ rpm ($0 - 112$ s). The roll contact had to be removed shortly after 1270 rpm to prevent the break-down of the polymer cover; strong barring may be sustained only for a few minutes.

In Fig. 11(a) the acceleration level settles within the vicinity of 4 m/s^2. A long-term vibration cycle can also be identified. The barring amplitude does not grow infinitely due to the nonlinear behavior of the cover contact in the nip. Increasing vibration intensifies the deformation of the polymer cover, causing the nip to widen, which leads to higher cover stiffness and damping, limiting the growth of the vibration amplitude. Small temperature changes synchronized with the change of the vibration amplitude were observed on the

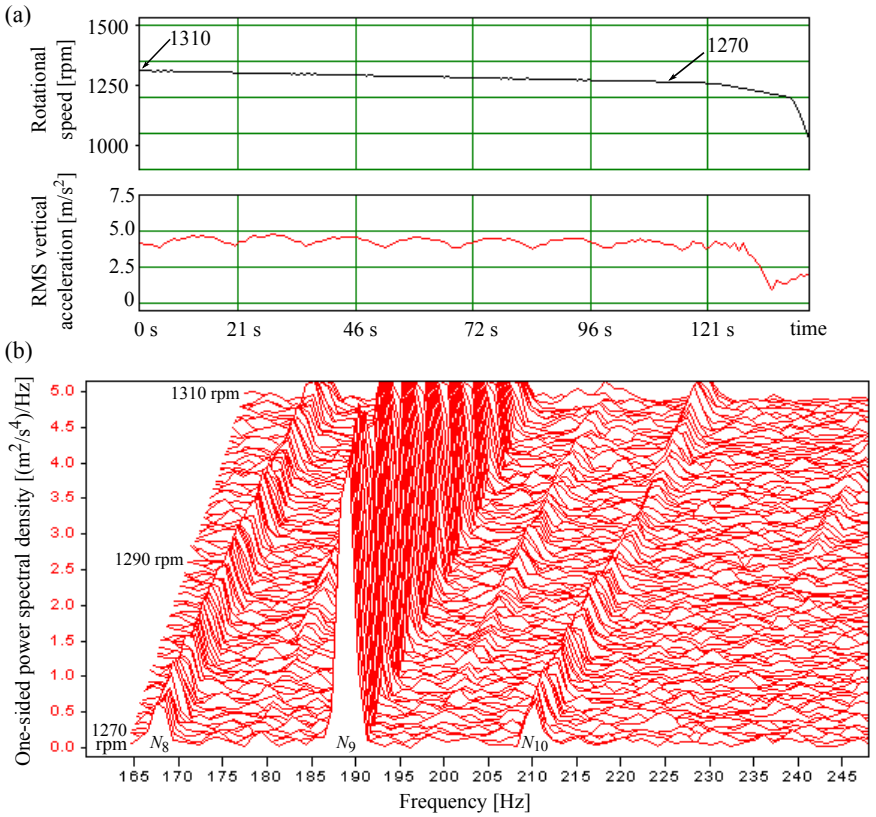

Figure 11: (a) Rotational speed of the upper roll and its vibration signal, i.e., the measured root-mean-square vertical acceleration. (b) Real-time power spectrum as a function of time calculated from the acceleration signal between $1310 \ldots 1270$ rpm ($0 - 112$ s). At 1310 rpm, time has been set to zero. The polygonal numbers related to the peaks are shown in the figure. At 1270 rpm, the primary peak corresponding to N_9 is located at 189 Hz and the secondary peaks corresponding to N_8 and N_{10} at 167 Hz and 210 Hz, respectively.

surface of the polymer cover. A growing amplitude leads to increasing temperature, which changes the cover stiffness and damping in the nip, creating a non-resonance condition. Consequently, the vibration amplitude and cover temperature begin to fall creating opposite changes in the cover stiffness and damping, thus increasing the amplitude and temperature again. Therefore, the long-term vibration cycle may be a consequence of the coupled thermal-mechanical behavior of the polymer cover.

It can be seen from Fig. 11(a) that the maximum vibration acceleration is reached around the rotational speed 1300 rpm. After this, the acceleration has a lowering trend, which indicates that the instability is weakening. In Fig. 11(b) the primary peaks in the spectrum lie in the vicinity of 190 Hz. In particular, at the rotational speeds 1310 and 1270 rpm the primary peaks lie at 194 and 189 Hz, respectively, exhibiting a lowering trend for decreasing rotational speed similarly to the calculated results of Figs. 10(a) and 10(b). If the polygonal numbers corresponding to the primary peaks are calculated by dividing the frequencies of the peaks by the corresponding revolution frequencies (21.83 and 21.17 Hz), we get 8.89 and 8.93, respectively. The result is in concordance with the behavior of N_9 in Fig. 4 in the sense that the polygonal number grows as the revolution frequency decreases.

Fig. 11(b) also displays smaller peaks in the spectrum, which at 1270 rpm are located at 210 and 167 Hz. These peaks indicate the existence of the deformation patterns pertaining to the polygonal numbers N_{10} and N_8, respectively. Based on the numerical computations, the instability areas of N_{10}, N_9 and N_8 lie in the range of $1146 - 1182$, $1272 - 1326$ and $1434 - 1506$ rpm, respectively. During the run-up from 0 to 1500 rpm, the system was driven in these areas approximately for 20, 30 and 40 s, respectively. During the short run-down from 1500 to 1400 rpm, before the actual experiment, the system was driven in the instability area

of N_8 for 20 s. Incipient barring corresponding to these polygonal numbers emerged when their instability areas were crossed. However, due to the fast speed change used when running these ramps, the steady formation of the polygonal deformation pattern was suppressed. Although barring did not develop to its full extent, minor deformation patterns remained on the cover when these areas were crossed. From 1400 rpm, the rotational speed was lowered slowly to 1270 rpm. Below 1330 rpm, the vibrations started to grow rapidly, and a fully-developed barring was formed in 30 s. It is evident that the pattern related to N_9, generated during the run-up stage, acted as a favourable initial condition for the barring vibrations corresponding to N_9, which blew up rapidly, while those corresponding to N_{10} and N_8 continued to fade away slowly. In the numerical calculations the viscoelastic memory was accounted for only from the previous period. Therefore, in Fig. 9 the polygonal patterns corresponding to N_{11} and N_{10} vanish before the instability zone of N_9 is reached, whereas in the real experiment (Fig. 11(b)) small secondary wave patterns (N_{10} and N_8) co-existed with the primary one (N_9). It should be noted, however, that the secondary wave patterns, which are stable within the speed interval under consideration, will vanish in time and have a minor effect on the system behavior.

In conclusion, the model shown in Fig. 1 can be used to locate the unstable and stable zones of the system fairly accurately and to explain the primary phenomena related to barring in a physically logical manner. The comparison between numerical and experimental results acts as motivation for further development of the model presented in this paper.

5. Conclusions

In this study, the viscoelastic memory effect of a polymer roll cover and the unstable vibrations induced by it in a two-roll system were investigated. The memory, formulated in a new way in this paper, introduced a time delay into the roll system. Thus the equations of motion of the system constituted a set of delay differential equations.

The calculated results displayed various moving surface patterns appearing on the roll cover and instability regions, which emerged when the frequency of the deformation pattern related excitation lay in the vicinity of the higher eigenfrequency of the system. On the basis of stability analysis, it was found that only one eigensolution of the system was unstable at a time. Therefore, comprehensive conclusions on the behavior of the roll system could be drawn based solely on the stability analysis and individual roots of the characteristic equation of the system. The phase-angle relation between the nip gap and viscous deformation played a key role in interpreting the phenomena related to the instability of the system. It was also shown that the values of the eigenfrequencies of the system may vary depending on the calculation method used, thus care ought to be taken when interpreting the results in relation to the eigenfrequencies. The roll support damping could be used as a countermeasure to diminish the harmful vibrations. By using a speed-up ramp, it was demonstrated that the instability regions of the system widened as the speed increased. At high speeds these regions may become too wide and unstable to be crossed in industrial machines. The calculated results were found to be in good concordance with the experimental results.

By using the SLS model and the retarded relaxation for the polymer cover, a general description of the dynamics of the system was formed. A simple model, which enables versatile analysis, may prove to be useful when designing vibration suppression for nipped roll systems.

References

[1] A. Sueoka, T. Ryu, T. Kondou, Y. Tsuda, K. Katayama, K. Takasaki, M. Yamaguchi, H. Hirooka, Polygonal deformation of roll-covering rubber, *JSME International Journal, Series C*, 39 (1) (1996) 1-10.

[2] A. Sueoka, T. Ryu, M. Yoshikawa, T. Kondou, Y. Tsuda, Pattern formation generated in a winder system of textile machine, *JSME International Journal, Series C*, 41 (3) (1998) 630-638.

[3] N. Sowa, T. Kondou, H. Mori, M.S. Choi, Method of preventing unstable vibration caused by time delays in contact rotating systems (application of new stability analysis), *JSME International Journal, Series C*, 49 (4) (2006) 973-982.

[4] M. Jorkama, R. von Hertzen, Delay phenomena in roll vibrations, *Proceedings of the VIII Finnish Mechanics Days*, June 2003, Espoo, Finland, pp. 111-121.

[5] M. Jorkama, R. von Hertzen, Two-drum winder stability analysis, *Pulp & Paper Canada*, 108 (5) (2007) 35-37.

[6] L.H. Yuan, Analysis of delay phenomena in roll dynamics, *Doctoral Thesis*, Tampere University of Technology, 2002.
[7] V.-M. Järvenpää, L.H. Yuan, Numerical modeling of paper machine roll contact with regenerative out-of-roundness excitation, In: P. Eberhard (Ed.), *IUTAM Symposium on Multiscale Problems in Multibody System Contacts*, Springer, 2007, pp. 55-64.
[8] L.H. Yuan, V.-M. Järvenpää, Nonlinear vibrations in a covered roll system with viscoelastic contact, *Communications in Nonlinear Science and Numerical Simulation*, 14 (7) (2009) 3170-3178.
[9] V.-M. Järvenpää, L.H. Yuan, Active vibration control of multibody rolling contact system, In: H. Ulbrich, L. Ginzinger (Eds.), *Motion and Vibration Control*, Springer, 2009, pp. 155-164.
[10] M. Hermanski, Barringbildung am Glättkalander einer Papiermaschine (Barring on the smoothing calender of a papermachine), *Das Papier*, 49 (6) (1995) 344-347.
[11] J. Karhunen, Elimination of self-excited resonance vibration in a size press through utilization of an automatically adjusting dynamic absorber, *Proceedings of the International Symposium on Multibody Systems and Mechatronics*, September 2002, Mexico City, Mexico, CD-ROM, 8p.
[12] K. Matzusaki, A. Sueoka, T. Ryu, H. Morita, Generation mechanism of polygonal wear of work rolls in a hot leveler and a countermeasure by dynamic absorbers, *International Journal of Machine Tools and Manufacture*, 48 (9) (2008) 983-993.
[13] K. Matzusaki, A. Sueoka, T. Ryu, H. Morita, K. Hidaka, S. Noguchi, Polygonal wear of work rolls in a hot leveler of a steel making machine (4th Report, Experimental verification of a countermeasure by using dynamic absorbers), *Journal of Environment and Engineering*, 3 (1) (2008) 146-157.
[14] T. Ryu, K. Matzusaki, A. Sueoka, H. Morita, Countermeasures against pattern formation phenomena of thin sheet winder by using dynamic absorbers, *Journal of System Design and Dynamics*, 3 (5) (2009) 814-826.
[15] T. Vuoristo, V.-T. Kuokkala, E. Keskinen, Dynamic compression testing of particle-reinforced polymer roll cover materials, *Composites: Part A*, 31 (8) (2000) 815-822.
[16] T. Vuoristo, V.-T. Kuokkala, E. Keskinen, Modeling of the deformation behavior of polymer composites at high strain rates and at elevated temperatures, *Key Engineering Materials*, 221-222 (2002) 221-232.
[17] T. Vuoristo, V.-T. Kuokkala, Creep, recovery and high strain rate response of soft roll cover materials, *Mechanics of Materials*, 34 (8) (2002) 493-504.
[18] T. Vuoristo, V.-T. Kuokkala, Effect of strain rate, moisture and temperature on the deformation behavior of polymer roll covers, *Experimental Mechanics*, 44 (3) (2004) 313-319.
[19] T. Vuoristo, Effect of strain rate on the deformation behavior of dual phase steels and particle reinforced polymer composites, *Doctoral Thesis*, Tampere University of Technology, 2004.
[20] F. Chinn, Dynamic instability of poly covered press rolls, *Pulp & Paper Canada*, 100 (1) (1999) 11-14.
[21] H. Rautiainen, J. Koriseva, R. Stapels, New vibration analysis tools optimize multi-nip calender operation, *Pulp & Paper Canada*, 101 (6) (2000) 151-154.
[22] I.M. Ward, J. Sweeney, *An Introduction to the Mechanical Properties of Solid Polymers*, John Wiley & Sons Ltd, Chichester, 2004.
[23] K.L. Johnson, *Contact Mechanics*, Cambridge University Press, Cambridge, 1987.
[24] D.J. Inman, *Engineering Vibration*, Prentice-Hall Inc., New Jersey, 2001.
[25] D.E. Müller, A method for solving algebraic equations using an automatic computer, *Mathematical Tables and Other Aids to Computation*, 10 (56) (1956) 208-215.
[26] R.D. Driver, *Ordinary and Delay Differential Equations*, Springer-Verlag, New York, 1977.